Frontiers of Physics
https://doi.org/10.1007/s11467-019-0892-5
Front. Phys.
14(4), 42502 (2019)

LETTER

Time-resolved imaging of mode-conversion process of terahertz transients in subwavelength waveguides

Yao Lu[1], Qiang Wu[1,†], Qi Zhang[1], Ri-De Wang[1], Bin Zhang[2,‡], Wen-Juan Zhao[1], Deng Zhang[1], Hao Xiong[1], Cheng-Liang Yang[3], Ji-Wei Qi[1], Chong-Pei Pan[1], Jing-Jun Xu[1]

[1] *The Key Laboratory of Weak-Light Nonlinear Photonics, Ministry of Education, TEDA Institute of Applied Physics and School of Physics, Nankai University, Tianjin 300457, China*
[2] *College of Science, Civil Aviation University of China, Tianjin 300300, China*
[3] *State Key Laboratory of Applied Optics, Changchun Institute of Optics, Fine Mechanics and Physics, Chinese Academy of Sciences, Changchun 130039, China*
Corresponding authors. E-mail: †*wuqiang@nankai.edu.cn,* ‡*b_zhang@cauc.edu.cn*
Received March 5, 2019; accepted March 10, 2019

We studied the mode-conversion process of terahertz pulses from a planar subwavelength waveguide to a tilted rectangular subwavelength waveguide. An unusual wavefront rotation, which led to an extra conversion time, was observed using a time-resolved imaging technique. We simulated the mode conversion process by a finite-difference time-domain method, and the results agreed well with the experiments. According to the simulations, the conversion time was demonstrated to become longer as the tilt angle or width of the rectangular waveguide increased. This work provides the possibility to optimize the future high-speed communications and terahertz integrated platforms.

Keywords ultrafast phenomenon, mode conversion, subwavelength waveguides, terahertz waves

1 Introduction

Recently, the increasing demands for broad communication bands and on-chip photonic communications require more studies on optics and photonics focusing on short/ultrashort pulses and micro/nano structures [1–4]. Thus, the studies on the behaviors of short/ultrashort light pulses in micro/nano structures become important. Classical guided-wave optics has clearly studied how the light propagates in subwavelength waveguides and some of the analyses can be inherited to study the behavior of pulsed light [5, 6]. These studies present the basis for many applications and much progress has been made. For example, a high-speed optical transceiver, which could achieve a very high-bandwidth optical interconnection and high-performance computing, was constructed using an on-chip integrated photonics/nanoelectronics platform [7]. In addition, photonic signal processing [8], coherent control and emission [9, 10] were also achieved. Especially, the on-chip mode (de)multiplexer has been consecutively improved to enable complicated and realistic photonic networks [11–13].

However, although the above-mentioned studies largely improved related applications and technologies, most of them failed to consider the transient behaviors of pulsed light in subwavelength waveguides. For instance, the mode-conversion process between different waveguides was hardly considered, which usually occurs and ends in several picoseconds or less, which requires a fine time-resolution detection. In addition, to understand this process need to solve the time-dependent solution of Maxwell equations, which could not be explained by the traditional geometrical optics or time-independent Helmholtz equation.

Besides, terahertz (THz) technology is gradually developing since it has presented outstanding and attractive performances in the fields of communication, imaging and sensing [14–17]. In recent years, increasingly more research has focused on the THz regime, such as subwavelength waveguides [5, 6], antennas [18, 19], metamaterials [20, 21], and microcavities [22, 23]. In particular, for the THz high-speed communication and on-chip integration, it is necessary to study the transient interactions between short/ultrashort THz pulses and subwavelength waveguides. Unfortunately, the related studies were seldom reported, which somehow limits the further development and update of the corresponding technologies.

In this article, we designed and manufactured two tilted rectangular subwavelength waveguides (RSWs) in a 50 μm-thick lithium niobite (LN) wafer. The short THz pulse with a duration of about a picosecond was generated in the sample by a femtosecond laser via impulsive stimulated Raman scattering [24, 25], which enables to integrate

the generation, control and propagation in a 50 μm-thick planar subwavelength waveguide (PSW), the LN sample. Using a time-resolved imaging technique, we recorded and studied the transient mode-conversion process of the THz pulses from a PSW to two RSWs with cross sections of 50 μm × 100 μm and 50 μm × 150 μm, individually. According to the experiments, an unusual wavefront rotation process was noted during the mode conversion. With the finite-difference time-domain (FDTD) simulation, we demonstrated that the wavefront rotation is caused by the tilt of RSW. Different performances of the mode-conversion process were also shown when we changed the tilt angle or width of the RSW. This work provides an insight to consider transient process. This finding is not only useful in THz technology but also in near infrared, especially in the mature technology, silicon photonics. Specifically, when a coupling device is designed to couple the light from one mode to another mode, the mode-conversion time needs to be considered. Otherwise, the steady mode may not form if an enough coupling length was not designed.

2 Experiments and results

In the experiment, the sample was produced using a 1 cm × 50 μm × 1.1 cm LN wafer with an optical axis parallel to the 1.1 cm-span boundary [z-axis in Fig. 1(a)]. The thickness of the sample is comparable to the wavelength of the THz waves so that it can be regarded as a PSW, in which two RSWs were fabricated via femtosecond-laser machining. During the fabrication process, the amplified Ti:sapphire laser-pulses (800 nm wavelength, 120 fs duration, 1 kHz repetition rate) with 5 μJ pulse energy, were focused by an objective with a numerical aperture of 0.25 to a spot size of about 4 μm. A three-dimensional translation stage held the 50 μm-thick LN slab. It was programmed to move laterally (about 0.4 mm/s), so that the outline of the air channel was irradiated and drilled, which was facilitated by moving the LN crystal along y direction. A scheme of the sample is shown in Fig. 1(a). Figure 1(b) shows the optical microscopy view for a part of the air channels. The outlines of the carved structure can be seen under illumination. As Figs. 1(a) and (b) show, a pair of 50 μm-wide parallel air channels was ablated from the wafer. This leaves two LN rods with cross sections of 50 μm × 100 μm and 100 μm × 150 μm to form two RSWs both with a tilt angle of $\alpha \approx 12°$ with respect to the x-axis [Fig. 1(a)].

THz waves were generated and detected by a pump-probe system [26]. Femtosecond laser pulses were divided into a pump beam (450 mW) and probe beam (50 mW). The pump pulses were directed to a mechanical time-delay line and then line-focused into the LN slab (a PSW), relatively far away from the RSW [Fig. 1(a)], using a cylindrical lens of 300 mm focal length, to generate THz waves [26, 27]. A scheme of the experimental setup is shown in Fig. 1(c). By gradually changing the optical path of the pump pulses, sequences of images of the THz waves were obtained [5, 26].

When the THz waves were generated in the PSW, they propagated along x-axis [Fig. 1(a)] as the modes of the PSW. Some of the THz waves entered the fabricated RSW and reached a new steady state, the mode of the RSW. Other THz waves did not enter the RSW and still propa-

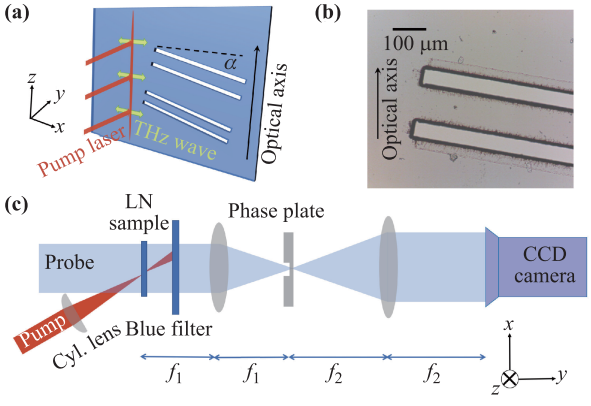

Fig. 1 **(a)** Schematic of the sample and the experimental setup. A femtosecond pump-laser was line-focused into the sample to generate THz waves. Both the coordinate system and optical-axis of the crystal are indicated in the figure. **(b)** Optical microscope image of the structure after the fabrication process. The LN sample is transparent under normal illumination, which reveals the outline of the carved structures. **(c)** Schematic of the setup. In the system, $f_1 = 10$ cm, $f_2 = 15$ cm.

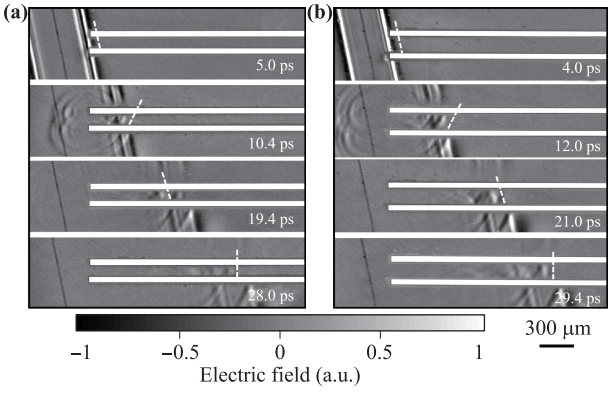

Fig. 2 Propagation of THz waves in the RSW structures. The experimental results recorded by a time-resolved phase-contrast method. **(a)** (Visualization 1) The cross section of the RSW is 50 μm × 100 μm. The pictures from top to bottom were recorded with a delay time of 5.0 ps, 10.4 ps, 19.4 ps, and 28.0 ps after the THz waves were generated. **(b)** (Visualization 2) The cross section of the RSW is 50 μm × 150 μm. The pictures from top to bottom were recorded with a delay time of 4.0 ps, 12.0 ps, 21.0 ps, and 29.4 ps after the THz waves were generated.

gated in the PSW. Figure 2 shows some images captured by the imaging system at different times, which enables an intuitive demonstration of the "wavefront rotation" of the THz wave during the mode-conversion process. Figures 2(a) and (b) show the mode-conversion process of THz waves from a 50 μm PSW to an RSW with cross sections of 50 μm × 100 μm (Visualization 1) and 50 μm × 150 μm (Visualization 2), respectively. As the THz pulse is launched and propagates in the PSW, it arrives at the critical boundary of the RSW. Due to the mismatch of the eigenmodes supported by RSW and PSW, mode conversion occurs. Interestingly, this process tends to be not just a simple rotation from a tilt (the wavefront in PSW) to a perpendicular direction (the wavefront in RSW). Instead, it behaves somewhat counterintuitive: the wavefront rotates beyond the steady-state position, which is perpendicular to the propagation direction, and then swings back to the initial side. After some pendulum-like swings, the wavefront stabilizes at its final steady-state position, i.e., a perpendicular wavefront.

3 FDTD simulations

To model the "wavefront rotation" phenomena, some 3D finite-difference time-domain (FDTD) calculations were performed. Standard perfect match layer was added as the boundary condition. The commercial software Lumerical FDTD Solutions provides an auto mesh module, which allows many models run correctly without specifically set the mesh grid size and time step. Simultaneously, to assign a specific mesh size which is smaller enough can also get the same results. In our settings, the mesh grid size was set automatically to level 3, which is about 4 μm for grid size and 15 fs for time step. This is a very fine mesh for THz waves centered at 0.5 THz, wavelength 600 μm in vacuum and about 2 ps for electromagnetic period, which guarantee the satisfaction of the Courant–Friedrichs–Levy condition. The geometric parameters and material parameters set according to our experiments [26, 27]. The conversion process are shown in Figs. 3(a) and (c), with the corresponding distributions of the Poynting vectors shown in Figs. 3(b) and (d), respectively. The simulations also show a wave rotation phenomenon, which agrees well with the experiments.

In order to clarify how the tilt of the RSW influenced the mode conversion, we simulated the conversion from a 50 μm PSW to an RSW with a cross sections of 50 μm × 100 μm but with different tilt angles. The material setting is the same as that used in Fig. 3. To be consistent with the experiments, the polarization and arrangement of the THz source were kept parallel to the optical axis of the LN material, when we changed the tilt angle. Figures 4(a) to (d) show the final steady state of the mode conversion in RSW with tilt angle of 0°, 10°, 20°, and 30°, respectively. Here, we determined the final steady state by the Poynting vectors. Specifically, when the leading Poynting vectors keep parallel to the propagation direction, the propagating was considered as a final steady state. For the non-tilt RSW, the wavefront does not rotate [Fig. 4(a)] and the conversion costs more time as the tilt angle increases. Figure 4(e) shows the dependence of time on tilt angle and the black dashed line show the time $t \approx 17$ ps at which nearly the whole THz pulse entered the RSW.

The mode conversion also costs different time when we change the width of the RSW. As Fig. 5 shows, the conversion time for RSWs with a width of 100 μm [Fig. 5(a)] and 150 μm [Fig. 5(b)]. The rectangular waveguide with widths of 250 μm [Fig. 5(c)] and 500 μm is non-subwavelngth for the THz waves centered at 0.5 THz

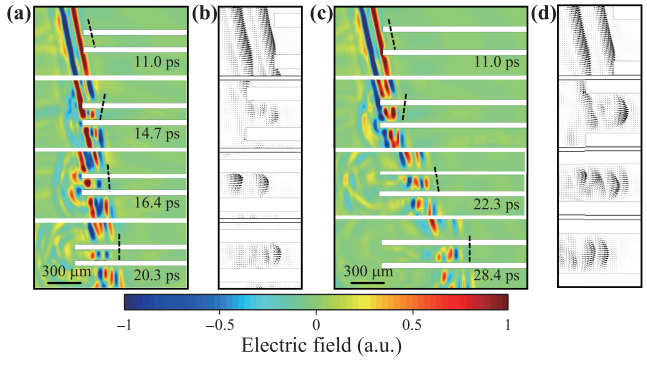

Fig. 3 FDTD simulations results of the experiments. **(a)** The cross section of the RSW is 50 μm × 100 μm. The pictures from top to bottom were recorded with a delay time of 11.0 ps, 14.7 ps, 16.4 ps, and 20.3 ps after the THz waves were generated. **(b)** Distributions of Poynting vectors of (a). **(c)** The cross section of the RSW is 50 μm × 150 μm. The pictures from top to bottom were recorded with a delay time of 11.0 ps, 15.2 ps, 22.3 ps, and 28.4 ps after the THz waves were generated. **(d)** Distributions of Poynting vectors of (c).

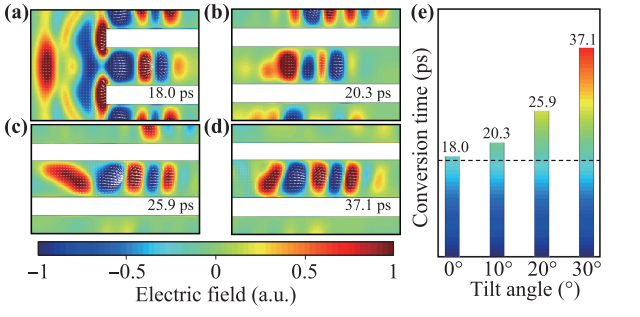

Fig. 4 Final steady states of mode-conversion of THz pulses from a PSW to an RSW with different tilt angles. The cross section of the RSW is 50 μm × 100 μm. **(a–d)** Final steady state for different tilt angles of $\alpha = 0°$, $\alpha = 10°$, $\alpha = 20°$, and $\alpha = 30°$. **(e)** Plot of the conversion time versus the tilt angle of the RSW. The black dashed line shows the time $t \approx 17$ ps when THz waves entered the RSW.

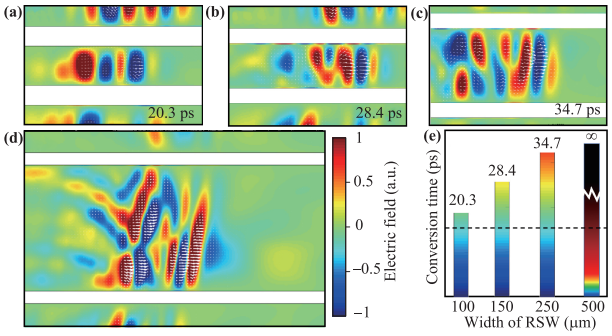

Fig. 5 Final states of mode-conversion of THz pulses with different widths of the rectangular waveguides. The tilt angle $\alpha = 10°$. **(a–d)** Final steady state for different widths of 100 μm, 150 μm, 250 μm, and 500 μm. **(e)** Plot of conversion time vesus width of the rectangular waveguide. The black dashed line shows the time $t \approx 17$ ps when THz waves entered the RSW.

in LN waveguide. Especially, when we increase the width of the RSW to 500 μm, the final steady state cannot be found anymore [Fig. 5(d)].

4 Analyses

All in all, the wavefront rotation can be observed in the subwavelength waveguide. In none-subwavelength waveguides, the wavefront rotation is replaced by an interference pattern [Fig. 5(d)]. To the best of our knowledge, this behavior is due to the reflection of THz waves near the boundary of the waveguide and the interference of the waves before and after the reflection. The THz waves were generated and transmitted into the rectangular waveguide before they reflected at the boundary of the waveguide. During the multiple reflections, the THz waves can be divided into two reflection modes: upwards reflection, and downwards reflection. When the THz waves are reflected, the two reflection modes can interfere near the boundary and form an interference pattern in the non-subwavelength waveguide [Fig. 5(d)]. Nevertheless, for the subwavelength condition, when the width of the waveguide decreases to subwavelength, a single interference spot is able to occupy the whole waveguide. Hence, a perpendicular wavefront is observed. According to the dispersion properties of the waveguides, the THz pulse has a larger phase velocity than its group velocity [5, 6]. Therefore, the energy seems to go backwards on the propagating wavefronts. As a result, the alternation of the two reflection modes was observed.

Generally speaking, the conversion time will be longer when the tilt angle is larger, which caused a larger mode mismatch, thus more time is needed to converse (Fig. 4). For the RSW with a larger width, it costs more time for the pulse to reach one boundary from the other one (Fig. 5). Therefore, either the width or the tilt angle of the RSW increases, the conversion time goes up correspondingly.

5 Conclusion

In conclusion, a mode-conversion process of THz pulses was experimentally observed and simulated in subwavelength waveguides. When the THz waves entered the tilted-RSW, an unexpected swing-like mode conversion process was noted. Furthermore, the time-dependent interference of the two reflected modes explains how the mode-conversion process occurs. We also found the wavefront rotation presents only in tilted subwavelength waveguides and behaves different when the tilt angles changes. In addition, the mode conversion process costs more time when we increase the tilt angle or the width of the rectangular waveguide. This study can advance the development of on-chip photonic platforms, and also provide some insight into transient phenomena in subwavelength waveguides, micro and nano optical devices, or integrated photonic platforms.

Acknowledgements This work was supported by the National Natural Science Foundation of China (NSFC) (Grant Nos. 61705013 and 61378018), the 111 Project (No. B07013), and the Program for Changjiang Scholars and Innovative Research Team in University (No. IRT_13R29).

References

1. W. Li, B. Chen, C. Meng, W. Fang, Y. Xiao, X. Li, Z. Hu, Y. Xu, L. Tong, H. Wang, W. Liu, J. Bao, and Y. R. Shen, Ultrafast all-optical graphene modulator, *Nano Lett.* 14(2), 955 (2014)
2. M. E. Fermann and I. Hartl, Ultrafast fiber laser technology, *IEEE J. Sel. Top. Quantum Electron.* 15(1), 191 (2009)
3. S. Sugiura and H. Iizuka, Deep-subwavelength MIMO using graphene-based nanoscale communication channel, *IEEE Access* 2, 1240 (2014)
4. L. R. Chen, J. Wang, B. Naghdi, and I. Glesk, Subwavelength grating waveguide devices for telecommunications applications, *IEEE J. Sel. Top. Quantum Electron.* 25(3), 8200111 (2019)
5. C. Yang, Q. Wu, J. Xu, K. A. Nelson, and C. A. Werley, Experimental and theoretical analysis of THz-frequency, direction-dependent, phonon polariton modes in a subwavelength, anisotropic slab waveguide, *Opt. Express* 18(25), 26351 (2010)
6. Y. Lu, Q. Wu, Q. Zhang, R. Wang, W. Zhao, D. Zhang, C. Pan, J. Qi, and J. Xu, Propagation of THz pulses in rectangular subwavelength dielectric waveguides, *J. Appl. Phys.* 123(22), 223103 (2018)
7. A. H. Atabaki, S. Moazeni, F. Pavanello, H. Gevorgyan, J. Notaros, L. Alloatti, M. T. Wade, C. Sun, S. A. Kruger,

and H. Meng, Integrating photonics with silicon nanoelectronics for the next generation of systems on a chip, *Nature* 556(7701), 349 (2018)

8. W. Zhang and J. Yao, A fully reconfigurable waveguide Bragg grating for programmable photonic signal processing, *Nat. Commun.* 9(1), 1396 (2018)
9. B. le Feber, N. Rotenberg, and L. Kuipers, Nanophotonic control of circular dipole emission, *Nat. Commun.* 6(1), 6695 (2015)
10. H. Shin, J. A. Cox, R. Jarecki, A. Starbuck, Z. Wang, and P.T. Rakich, Control of coherent information via on-chip photonic-phononic emitter-receivers, *Nat. Commun.* 6, 6427 (2015)
11. A. Y. Piggott, J. Lu, K. G. Lagoudakis, J. Petykiewicz, T. M. Babinec, and J. Vučković, Inverse design and demonstration of a compact and broadband on-chip wavelength demultiplexer, *Nat. Photon.* 9, 374 (2015)
12. Y. Tan, H. Wu, S. Wang, C. Li, and D. Dai, Silicon-based hybrid demultiplexer for wavelength- and mode-division multiplexing, *Opt. Lett.* 43(9), 1962 (2018)
13. D. Dai, C. Li, S. Wang, H. Wu, Y. Shi, Z. Wu, S. Gao, T. Dai, H. Yu, and H. K. Tsang, 10-channel mode (de)multiplexer with dual polarizations, *Laser Photon. Rev.* 12(1), 1700109 (2018)
14. S. Koenig, D. Lopezdiaz, J. Antes, F. Boes, R. Henneberger, A. Leuther, A. Tessmann, R. Schmogrow, D. Hillerkuss, R. Palmer, T. Zwick, C. Koos, W. Freude, O. Ambacher, J. Leuthold, and I. Kallfass, Wireless sub-THz communication system with high data rate, *Nat. Photon.* 7(12), 977 (2013)
15. S. S. Dhillon, M. S. Vitiello, E. H. Linfield, A. G. Davies, M. C. Hoffmann, J. Booske, C. Paoloni, M. Gensch, P. Weightman, G. P. Williams, E. Castro-Camus, D. R. S. Cumming, F. Simoens, I. Escorcia-Carranza, J. Grant, S. Lucyszyn, M. Kuwata-Gonokami, K. Konishi, M. Koch, C. A. Schmuttenmaer, T. L. Cocker, R. Huber, A. G. Markelz, Z. D. Taylor, V. P. Wallace, J. Axel Zeitler, J. Sibik, T. M. Korter, B. Ellison, S. Rea, P. Goldsmith, K. B. Cooper, R. Appleby, D. Pardo, P. G. Huggard, V. Krozer, H. Shams, M. Fice, C. Renaud, A. Seeds, A. Stöhr, M. Naftaly, N. Ridler, R. Clarke, J. E. Cunningham, and M. B. Johnston, The 2017 terahertz science and technology roadmap, *J. Phys. D Appl. Phys.* 50(4), 043001 (2017)
16. D. L. Woolard, R. Brown, M. Pepper, and M. Kemp, Terahertz frequency sensing and imaging: A time of reckoning future applications? *Proc. IEEE* 93(10), 1722 (2005)
17. A. G. Davies, A. D. Burnett, W. Fan, E. H. Linfield, and J. E. Cunningham, Terahertz spectroscopy of explosives and drugs, *Mater. Today* 11(3), 18 (2008)
18. A. Zak, M. A. Andersson, M. Bauer, J. Matukas, A. Lisauskas, H. G. Roskos, and J. Stake, Antenna-integrated 0.6 THz FET direct detectors based on CVD graphene, *Nano Lett.* 14(10), 5834 (2014)
19. Q. Zhang, J. Qi, Q. Wu, Y. Lu, W. Zhao, R. Wang, C. Pan, S. Wang, and J. Xu, Surface enhancement of THz wave by coupling a subwavelength $LiNbO_3$ slab waveguide with a composite antenna structure, *Sci. Rep.* 7(1), 17602 (2017)
20. G. Scalari, C. Maissen, D. Turcinkova, D. Hagenmuller, S. De Liberato, C. Ciuti, C. Reichl, D. Schuh, W. Wegscheider, M. Beck, and J. Faist, Ultrastrong coupling of the cyclotron transition of a 2D electron gas to a THz metamaterial, *Science* 335(6074), 1323 (2012)
21. B. Zhang, Q. Wu, C. Pan, R. Feng, J. Xu, C. Lou, X. Wang, and F. Yang, THz band-stop filter using metamaterials surfaced on $LiNbO_3$ sub-wavelength slab waveguide, *Opt. Express* 23(12), 16042 (2015)
22. P. Sivarajah, A. Steinbacher, B. Dastrup, and K. Nelson, THz-frequency cavity magnon-phonon-polaritons in the strong coupling regime, arXiv: 1707.03503 (2017)
23. C. Pan, Q. Wu, Q. Zhang, W. Zhao, J. Qi, J. Yao, C. Zhang, W. T. Hill, and J. Xu, Direct visualization of light confinement and standing wave in THz Fabry–Perot resonator with Bragg mirrors, *Opt. Express* 25(9), 9768 (2017)
24. T. P. Dougherty, G. P. Wiederrecht, K. A. Nelson, M. H. Garrett, H. P. Jensen, and C. Warde, Femtosecond resolution of soft mode dynamics in structural phase transitions, *Science* 258(5083), 770 (1992)
25. T. P. Dougherty, G. P. Wiederrecht, and K. A. Nel-son, Impulsive stimulated Raman scattering experiments in the polariton regime, *J. Opt. Soc. Am. B* 9(12), 2179 (1992)
26. Q. Wu, C. A. Werley, K. H. Lin, A. Dorn, M. G. Bawendi, and K. A. Nelson, Quantitative phase contrast imaging of THz electric fields in a dielectric waveguide, *Opt. Express* 17(11), 9219 (2009)
27. C. H. Henry and J. J. Hopfield, Raman scattering by polaritons, *Phys. Rev. Lett.* 15, 964 (1965)